Numerical dispersion in Eulerian-Lagrangian methods

Thomas F. Russell[a*]

[a]Department of Mathematics, University of Colorado at Denver,
P.O. Box 173364, Campus Box 170, Denver, CO 80217-3364, U.S.A.

The common "folklore" that Eulerian-Lagrangian methods perform better (are more accurate) with large Courant numbers (large time steps) than with small Courant numbers, due to numerical dispersion in the latter case, is explained theoretically. A formulation that does not suffer from large numerical dispersion for any Courant number is outlined.

1. INTRODUCTION

There appears to be a certain amount of misunderstanding in the hydrological modeling community of the extent to which Eulerian-Lagrangian methods (ELMs) for advection-dispersion transport equations are numerically dispersive. One often hears that ELMs perform well for problems in which they can successfully use a large Courant number (large time step), but that when forced to use a smaller Courant number, and hence more time steps, they suffer from numerical dispersion introduced by interpolation at each step. Indeed, some formulations of ELMs behave in precisely this way, and the implementation and use of such formulations has probably contributed to this perception. What is less well understood is that other formulations can avoid or substantially mitigate this effect.

The key to the situation is the relationship between averaging in the mass matrix and averaging in the right-hand-side vector. The mass matrix represents the discrete storage terms at the new time level. In the right-hand-side vector, advected old-time values are averaged by interpolation or some analogous process such as numerical integration. If the averaging on these two sides is balanced, then fronts can be propagated with minimal numerical dispersion, regardless of the time step. In numerically dispersive formulations, the mass matrix is typically "lumped," i.e., diagonal, meaning that there is no averaging in the mass matrix to balance the averaging on the right-hand side.

This paper will detail the theoretical basis for this discussion, outline a non-dispersive formulation, and discuss the expected behavior of various formulations of ELMs in some simple cases.

2. A SIMPLE EULERIAN-LAGRANGIAN METHOD

The concepts to be discussed in this paper are most easily and clearly presented in the context of a 1-D constant-coefficient advection-dispersion equation, where there are no

*This research was supported in part by NSF Grants DMS-9706866 and DMS-0084438 and ARO Grant 37119-GS-AAS.

extraneous features. Consider the model problem

$$\mathcal{L}u \equiv u_t + Vu_x - Du_{xx} \equiv u_\tau - Du_{xx} = f(x,t), \quad 0 < x < L, \quad t > 0, \tag{1}$$

with appropriate initial and boundary conditions that are not relevant here. For the sake of simplicity, define a uniform grid with $\Delta x = L/I$, nodes $x_i = i\Delta x$ $(i = 0, 1, \ldots, I)$, and cells $C_i = [x_{i-1/2}, x_{i+1/2}] = [(i-1/2)\Delta x, (i+1/2)\Delta x]$ centered around the nodes. Similarly, define a time increment Δt, uniform time levels $t^n = n\Delta t$ $(n = 0, 1, 2, \ldots)$, and time intervals $J^n = [t^n, t^{n+1}]$.

The space-time τ-directional derivative in (1) is a total (or Lagrangian, substantial, or material) derivative that follows the advective part of the flow. Along this direction, with the point (x, t^{n+1}) we associate the point (x^*, t^n) at the previous time level that flows to (x, t^{n+1}) under advection (see Figure 1), namely

$$x^* = x - V\Delta t. \tag{2}$$

We can then make a backward-Euler approximation of the total derivative,

$$u_\tau(x, t^{n+1}) \approx \frac{u(x, t^{n+1}) - u(x^*, t^n)}{\Delta t}. \tag{3}$$

Incorporating (2) and (3) into a centered implicit finite-difference method (FDM) for (1), in the interior we have the finite-difference Eulerian-Lagrangian method (FDELM)

$$\frac{U_i^{n+1} - U^n(x_i^*)}{\Delta t} + D\frac{-U_{i-1}^{n+1} + 2U_i^{n+1} - U_{i-1}^{n+1}}{\Delta x^2} = f_i^{n+1}, \tag{4}$$

where U is the FDELM approximation to u, $U_i^{n+1} = U(x_i, t^{n+1})$, and $f_i^{n+1} = f(x_i, t^{n+1})$. Let $\delta_x^2 U_i = U_{i-1} - 2U_i + U_{i+1}$ denote the second spatial difference operator and I the identity operator, and rewrite (4) in the form

$$\left(I - D\frac{\Delta t}{\Delta x^2}\delta_x^2\right) U_i^{n+1} = U^n(x_i^*) + \Delta t f_i^{n+1}. \tag{5}$$

Complete specification of the interior FDELM (5) requires evaluation of the solution at the old time level, $U^n(x_i^*) = U^n(x_i - V\Delta t)$. Because x_i^* does not lie at a node in general (see Figure 1), some form of interpolation or the equivalent is needed.

Let Cr denote the Courant number,

$$Cr = V\Delta t/\Delta x, \tag{6}$$

which is the number of cells traversed by advection in one time step. For definiteness, assume that $Cr \geq 0$, and denote its integer and fractional parts by $[Cr]$ and (Cr), respectively. The simplest evaluation of $U^n(x_i^*)$ is by linear interpolation,

$$U^n(x_i^*) = U^n(x_i - Cr\Delta x) = (1 - (Cr))U_{i-[Cr]}^n + (Cr)U_{i-[Cr]-1}^n. \tag{7}$$

Consider the case $0 \leq Cr < 1$ ($[Cr] = 0$, $(Cr) = Cr$), substitute (7) into (5), and use (6) to obtain

$$\left(I - D\frac{\Delta t}{\Delta x^2}\delta_x^2\right) U_i^{n+1} + \Delta t V\frac{U_i^n - U_{i-1}^n}{\Delta x} = U_i^n + \Delta t f_i^{n+1}; \tag{8}$$

in (8) we have precisely a first-order explicit upwind FDM in the advection term. This shows that: *For $0 \le Cr \le 1$, the FDELM (5) reduces to the first-order explicit upwind FDM (8).* This method is known to be numerically dispersive.

To quantify the numerical dispersivity of (8), rewrite it in the form of a second-order centered FDM plus a numerical dispersion term [1]:

$$\left(I - D\frac{\Delta t}{\Delta x^2}\delta_x^2\right) U_i^{n+1} + \Delta t V \frac{U_{i+1}^n - U_{i-1}^n}{2\Delta x} - D_{num}\frac{\Delta t}{\Delta x^2}\delta_x^2 U_i^n = U_i^n + \Delta t f_i^{n+1}, \tag{9}$$

where we have determined the *numerical dispersivity*

$$D_{num} = V\Delta x/2. \tag{10}$$

3. DISCUSSION

It is possible for the FDELM (5) to be less dispersive and more accurate with larger time steps, $Cr > 1$. In such a case, in a time step the solution is advected $[Cr]$ cells without dispersion, then is evolved by the upwind FDM to complete the time step. Because fewer interpolations (upwind steps) are needed for a given simulation time as the time step is increased, the resulting U is less dispersed. This effect is balanced by increasing errors in the physical dispersion approximation and the source term as Δt increases, so that it is plausible to seek an "optimal time step" that minimizes the sum of the advective and dispersive errors [2]. This example, and others similar to it, appear to be the reason for the "folklore" mentioned in the abstract and introduction.

Within the framework of (5), numerical dispersion can be avoided by a form of quadratic interpolation, as proved in [3]. There a second-order error estimate was demonstrated, a consequence of which is that first-order numerical dispersion must be absent. Rather than pursuing that line of reasoning further, here we will consider finite-volume ELMs that can alleviate the numerical dispersion in a systematic way that is relatively straightforward to understand.

Neglecting the physical dispersion in (5), the identity operator is applied to U^{n+1}, and an interpolation operator to U^n. The net effect is that the solution U^{n+1} will be some type of weighted average of U^n. With higher-order interpolation as in [3], negative weights will be necessary if numerical dispersion is to be avoided, creating the potential for spurious oscillations. Nonlinear interpolators that combine linear and quadratic techniques or other combinations, such as slope limiters, can be used [4]. These are more difficult to formulate in multiple dimensions and near boundaries. In ELMs that often reach to or across boundaries in determining the backtracked point x^* in (2), we have found it natural and advantageous to modify the treatment of the left-hand side of (5), rather than the right-hand side. This will be described in the context of a finite-volume Eulerian-Lagrangian localized adjoint method (FVELLAM) [5,6].

4. FINITE-VOLUME ELLAM

The Eulerian-Lagrangian localized adjoint method (ELLAM) [7] uses space-time finite elements oriented along the τ directional derivative of (1), generalizing ELMs in a mass-conservative way that systematically treats general boundary conditions. This is one

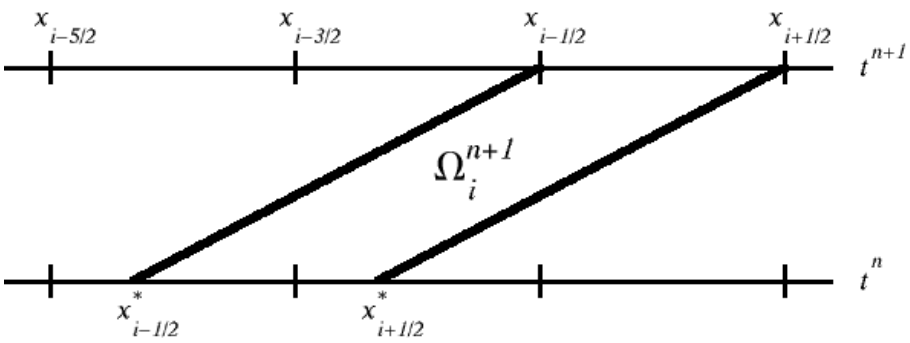

Figure 1. An FVELLAM space-time cell.

of many possible settings for the ensuing discussion, but seems to provide some insight on possible treatments of numerical dispersion. The FVELLAM uses space-time test functions that are characteristic (indicator) functions of space-time subdomains oriented along τ. This will be described briefly here to set the stage.

As in Figure 1, define the cell $C_i = [x_{i-1/2}, x_{i+1/2}]$ at the new time level t^{n+1}, and its backtracked image $C_i^* = [x^*_{i-1/2}, x^*_{i+1/2}]$ at t^n, and the space-time cell Ω_i^{n+1} that consists of all points between them. A discrete interior FVELLAM equation (we do not consider boundary issues here) is obtained by integrating (1) over Ω_i^{n+1} in space and time, or equivalently by multiplying (1) by the characteristic function of Ω_i^{n+1} and integrating over the whole space-time domain. In the integration, note that the measures $dx\,dt$ and $dx\,d\tau$ are the same, so that we can think of "time" integration in the τ direction instead of t. So doing, we obtain

$$\int_{\Omega_i^{n+1}} u_\tau \, d\tau \, dx - \int_{\Omega_i^{n+1}} D u_{xx} \, dx \, d\tau = \int_{\Omega_i^{n+1}} f \, dx \, d\tau, \tag{11}$$

and integrating in τ and x, respectively, in the first two terms of (11),

$$\begin{aligned} &\int_{x_{i-1/2}}^{x_{i+1/2}} u^{n+1}(x)\, dx + D \int_{t^n}^{t^{n+1}} [u_x(x_{i-1/2} - V(t^{n+1} - \tau), \tau) - u_x(x_{i+1/2} - V(t^{n+1} - \tau), \tau)]\, d\tau \\ &= \int_{x^*_{i-1/2}}^{x^*_{i+1/2}} u^n(x^*)\, dx^* + \int_{\Omega_i^{n+1}} f \, dx \, d\tau. \end{aligned} \tag{12}$$

The FVELLAM is obtained by choosing approximations U^n and U^{n+1} for u^n and u^{n+1}, and numerical integration rules in (12). We use a backward-Euler approximation of the time integrals, so that (12) is approximated by

$$\begin{aligned} &\int_{x_{i-1/2}}^{x_{i+1/2}} U^{n+1}(x)\, dx + D\Delta t[(U_x)^{n+1}_{i-1/2} - (U_x)^{n+1}_{i+1/2}] \\ &= \int_{x^*_{i-1/2}}^{x^*_{i+1/2}} U^n(x^*)\, dx^* + \Delta t \int_{x_{i-1/2}}^{x_{i+1/2}} f^{n+1}(x)\, dx. \end{aligned} \tag{13}$$

The crux of our discussion is the evaluation of the U^{n+1} integral on the left-hand side of (13) and the U^n integral on the right-hand side.

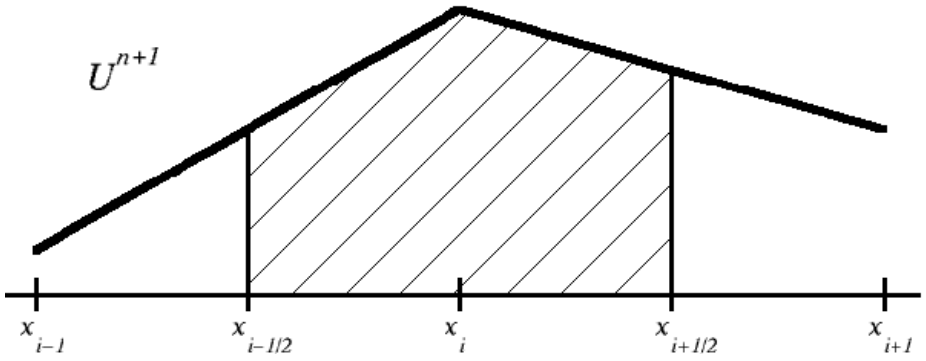

Figure 2. Area showing value of left-hand-side U^{n+1} integral.

4.1. U^{n+1} integral

In a finite-volume method, it is customary to think of the solution U^{n+1} as piecewise-constant, i.e., constant on each spatial cell C_i. This choice would lead to (5), and hence to the same numerical dispersion noted there. Instead we view U^{n+1} as piecewise-linear, interpolated between nodes x_i. The U^{n+1} integral in (13) is then the area depicted in Figure 2, which is

$$\int_{x_{i-1/2}}^{x_{i+1/2}} U^{n+1}(x)\,dx = \Delta x \left(\frac{1}{8}U_{i-1}^{n+1} + \frac{3}{4}U_i^{n+1} + \frac{1}{8}U_{i+1}^{n+1}\right) = \Delta x \left(I + \frac{1}{8}\delta_x^2\right) U_i^{n+1}. \tag{14}$$

In comparison with (5), the weights 1/8, 3/4, 1/8 in (14) "unlump" the left-hand side of (13). If we approximate U_x by a difference quotient and f^{n+1} by a piecewise-constant function, we can write (13) in the form analogous to (9),

$$\Delta x \left(I - \left(D - \frac{1}{8}\frac{\Delta x^2}{\Delta t}\right)\frac{\Delta t}{\Delta x^2}\delta_x^2\right) U_i^{n+1} = \int_{x_{i-1/2}^*}^{x_{i+1/2}^*} U^n(x^*)\,dx^* + \Delta x \Delta t f_i^{n+1}. \tag{15}$$

We see that unlumping has introduced in (15) a *negative* numerical dispersivity

$$D_{num} = -\frac{1}{8}\frac{\Delta x^2}{\Delta t}. \tag{16}$$

4.2. U^n integral

The key to alleviating numerical dispersion in FVELLAM is to balance the negative dispersivity of unlumping with positive dispersivity in the evaluation of the U^n integral in (13). The unlumping has created "room" for a weighted average, or equivalently a numerical integration, in the U^n integral to be non-dispersive in the end. The following discussion is directed toward achieving the desired balance.

For the simple problem considered here, exact integration is possible, evaluating $U^n(x^*)$ as in (7) in terms of the Courant number Cr. For $0 \le Cr \le 1/2$, $C_i^* = [x_{i-1/2}^*, x_{i+1/2}^*] \subset [x_{i-1}, x_{i+1}]$, so that a single formula in terms of U_{i-1}^n, U_i^n, and U_{i+1}^n is applicable. A complementary formula covers the case $1/2 \le Cr \le 1$, and simple shifts incorporate the integer part $[Cr]$. For $0 \le Cr \le 1/2$, straightforward algebra yields

$$\int_{x_{i-1/2}^*}^{x_{i+1/2}^*} U^n(x^*)\,dx^* \;=\; \Delta x \left(\left(\frac{1}{8} + \frac{Cr}{2} + \frac{Cr^2}{2}\right) U_{i-1}^n + \left(\frac{3}{4} - Cr^2\right) U_i^n\right.$$

$$+\left(\frac{1}{8}-\frac{Cr}{2}+\frac{Cr^2}{2}\right)U_{i+1}^n\Bigg). \tag{17}$$

For $Cr=0$, the weights 1/8, 3/4, 1/8 reappear, properly balancing the left-hand side. In practice, numerical integration will be necessary, so we seek a quadrature formula that balances well over a range of Courant numbers.

To conserve global mass in the U^n integral, in general it is necessary to evaluate the integral with a forward-tracking procedure [8,5]. Quadrature points are regularly distributed at t^n, hence integrate the total mass exactly. Each point is tracked forward to t^{n+1}, and if it lands in $C_i=[x_{i-1/2},x_{i+1/2}]$, its mass is then contributed to the integral over $C_i^*=[x_{i-1/2}^*,x_{i+1/2}^*]$. With discontinuous characteristic functions as in Figure 1, the numerical integral can be changed greatly by small changes in Cr. For example, with quadrature points $x_{i-1},x_{i-1/2},x_i,x_{i+1/2},x_{i+1}$ each carrying mass (domain length) $\Delta x/2$, the U^n integral in (13) will be approximated by $\Delta x(1/4\ U_{i-1}^n+3/4\ U_i^n)$ if Cr is small and positive, but by $\Delta x(3/4\ U_i^n+1/4\ U_{i+1}^n)$ if Cr is small and negative. This discontinuous sensitivity will yield unacceptable results in practice, so for numerical purposes it is necessary to modify the integral with a continuous smoothed test function:

$$\int_{x_{i-1/2}^*}^{x_{i+1/2}^*}U^n(x^*)\,dx^*\approx\int_0^L U^n(x^*)W_i(x^*,t^n)\,dx^*, \tag{18}$$

where $W_i(x^*,t^n)$ is a continuous approximation of the discontinuous characteristic function of C_i^*. A natural first choice is to take $W_i(x,t^{n+1})$ to be the piecewise-linear hat function equal to 1 at x_i and 0 at all other nodes, and let $W_i(x^*,t^n)=W_i(x,t^{n+1})$.

The piecewise-linear W_i makes the integrand on the right-hand side of (18) piecewise-quadratic. If integrated exactly, it will produce weights of 1/6, 2/3, 1/6 (the weights of Simpson's rule) for $Cr=0$. These do not match the desired 1/8, 3/4, 1/8. In a manner analogous to (16), a right-hand-side $D_{num}=1/6\ \Delta x^2/\Delta t$ results, hence an overall numerical dispersivity

$$D_{num}=\left(\frac{1}{6}-\frac{1}{8}\right)\frac{\Delta x^2}{\Delta t}=\frac{1}{24}\frac{\Delta x^2}{\Delta t}. \tag{19}$$

For fixed Δx and small Δt, results will be excessively dispersed.

Thus, if W_i is used, we must integrate approximately in a fashion that restores the weights 1/8, 3/4, 1/8 of the exact non-W_i integral for the case $Cr=0$. Comparing Figure 3 to the exact non-W_i area in Figure 2, the shaded areas are the same, and the shaded area in Figure 3 would be obtained from the trapezoidal rule, with $W_i(x_{i-1})=0$, $W_i(x_{i-1/2})=1/2$, $W_i(x_i)=1$, $W_i(x_{i+1/2})=1/2$, and $W_i(x_{i+1})=0$. For $0\le Cr\le 1/2$ with the trapezoidal rule, we have

$$\begin{aligned}\int_0^L U^n(x^*)W_i(x^*,t^n)\,dx^* &\approx \Delta x\left(\left(\frac{1}{8}+\frac{3}{4}Cr\right)U_{i-1}^n+\left(\frac{3}{4}-\frac{Cr}{2}\right)U_i^n+\left(\frac{1}{8}-\frac{Cr}{4}\right)U_{i+1}^n\right)\\ &= \int_{x_{i-1/2}^*}^{x_{i+1/2}^*}U^n(x^*)\,dx^*+\Delta x\left(\frac{Cr}{4}-\frac{Cr^2}{2}\right)\delta_x^2U_i^n,\end{aligned} \tag{20}$$

by (17). Analogous to (19), the overall numerical dispersivity is

$$D_{num}=\left(\frac{1}{4}Cr-\frac{1}{2}Cr^2\right)\frac{\Delta x^2}{\Delta t}=\frac{V\Delta x}{4}-\frac{V^2\Delta t}{2}. \tag{21}$$

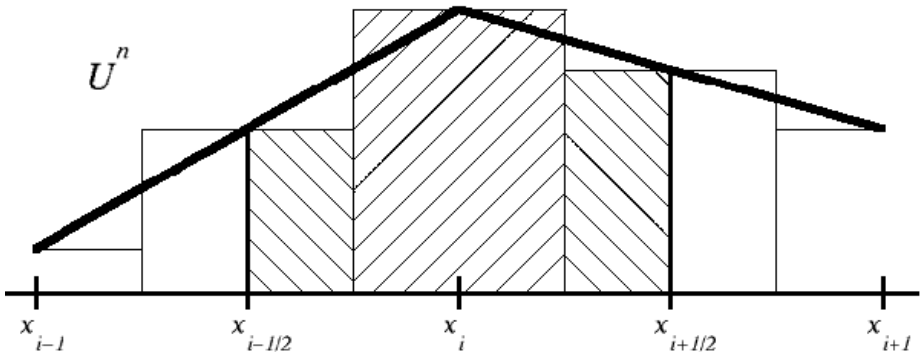

Figure 3. Trapezoidal rule to determine correct area, $Cr = 0$, $NS = 2$.

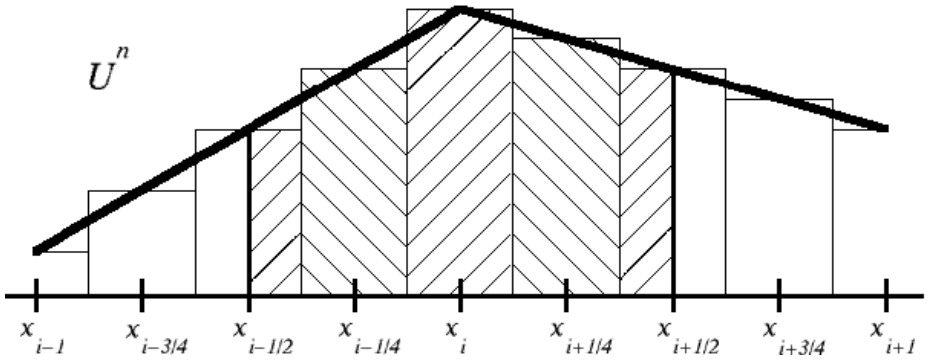

Figure 4. Trapezoidal rule to determine correct area, $Cr = 0$, $NS = 4$.

Unlike (19), as $\Delta t \longrightarrow 0$ the dispersivity in (21) has a finite limit $V\Delta x/4$, which is half of the numerical dispersivity of upwinding in (10). Note that the trapezoidal rule is calculated on a mesh of size $\Delta x/2$, compared to upwinding on size Δx in (8).

Numerical results were reported in Problem 1 of [5] for a test case with $V = 25$, $D = 2.5$, $\Delta x = 2$, $\Delta t = 0.001$ (cell Péclet number $Pe \equiv V\Delta x/D = 20$, $Cr = 1/80$), $L = 250$, final time 2. For these values, (21) gives $D_{num} = 12.2$, hence the total dispersivity of 14.7 is 5.9 times the physical dispersivity. Then the numerical front width should be about $\sqrt{5.9} \approx 2.4$ times the analytical front width. The widths between 95% and 5% concentration in the numerical and analytical solutions were $14\Delta x$ and $6\Delta x$, respectively. For the same data except that $\Delta t = 0.01$ ($Cr = 1/8$), hence $D_{num} = 9.375$, $D + D_{num} = 4.75D$, $\sqrt{4.75} \approx 2.2$, the numerical and analytical front widths were $10\Delta x$ and $5\Delta x$, respectively. This indicates that the analysis explains the dispersivity behavior very well.

As suggested by the comparison between (21) and (10), it is possible to reduce the dispersivity by using the trapezoidal rule on a finer set of quadrature points. Let NS be the number of subintervals in the cell C_i; in Figure 3, $NS = 2$. Figure 4 shows the case $NS = 4$. The exact area will be obtained as shown, if the values $W_i(x_{i-1}) = W_i(x_{i-3/4}) =$

0, $W_i(x_{i-1/2}) = 1/2$, $W_i(x_{i-1/4}) = W_i(x_i) = W_i(x_{i+1/4}) = 1$, $W_i(x_{i+1/2}) = 1/2$, and $W_i(x_{i+3/4}) = W_i(x_{i+1}) = 0$ are used (this is depicted in Figure 4 of [5]). Thus, instead of a hat function, W_i in this case changes linearly from 0 to 1 on $[x_{i-3/4}, x_{i-1/4}]$, and from 1 to 0 on $[x_{i+1/4}, x_{i+3/4}]$. A development similar to (20) concludes that

$$D_{num} = \left(\frac{1}{8}Cr - \frac{1}{2}Cr^2\right)\frac{\Delta x^2}{\Delta t} = \frac{V\Delta x}{8} - \frac{V^2\Delta t}{2} \longrightarrow \frac{V\Delta x}{8} \text{ as } \Delta t \longrightarrow 0. \tag{22}$$

More generally, for any even value of NS, we have $W_i(x_{i-1/2}) = W_i(x_{i+1/2}) = 1/2$, $W_i = 1$ at all quadrature points in between, $W_i = 0$ at all quadrature points outside, and W_i is interpolated linearly between quadrature points. With these specifications, D_{num} tends to the limit $V\Delta x/2NS$ as $\Delta t \longrightarrow 0$. Thus, with denser trapezoidal-quadrature points, numerical dispersivity can be made very small, even with small Courant number.

5. CONCLUSIONS

The observed numerical dispersion in Eulerian-Lagrangian methods (ELMs), particularly with small time steps, is not an intrinsic feature of ELMs. Rather, it is a result of formulations whose mass matrix is lumped, as is typical for finite differences. With an unlumped mass matrix, and careful balancing of it with the integration rule for the old-time-level mass, one can design ELMs that exhibit minimal numerical dispersion for any Courant number, large or small.

REFERENCES

1. D. W. Peaceman, Fundamentals of Numerical Reservoir Simulation, Elsevier, Amsterdam, 1977.
2. A.M. Baptista, Solution of advection-dominated transport by Eulerian-Lagrangian methods using backward methods of characteristics, PhD Dissertation, Dept. of Civil Engineering, MIT, 1987.
3. J. Douglas Jr. and T.F. Russell, Numerical methods for convection-dominated diffusion problems based on combining the method of characteristics with finite element or finite difference procedures, SIAM J. Numer. Anal. 19 (1982) 871.
4. R. J. LeVeque, Numerical Methods for Conservation Laws, Birkhäuser, Basel, 1992.
5. R.W. Healy and T.F. Russell, A finite-volume Eulerian-Lagrangian localized adjoint method for solution of the advection-dispersion equation, Water Resour. Res. 29 (1993) 2399.
6. P. Binning and M.A. Celia, A finite volume Eulerian-Lagrangian localized adjoint method for solution of the contaminant transport equations in two-dimensional multiphase flow systems, Water Resour. Res. 32 (1996) 103.
7. M.A. Celia, T.F. Russell, I. Herrera, and R.E. Ewing, An Eulerian–Lagrangian localized adjoint method for the advection-diffusion equation, Adv. Water Resour. 13 (1990) 187.
8. T. F. Russell and R. V. Trujillo, Eulerian-Lagrangian localized adjoint methods with variable coefficients in multiple dimensions, Computational Methods in Surface Hydrology, G. Gambolati et al. (eds.), Computational Mechanics Publications, Southampton, U.K., 1990, 357.